Design of Two-Dimensional Multiferroics with Direct Polarization-Magnetization Coupling

Junting Zhang,[1,*] Xiaofan Shen,[1] Yancheng Wang,[1] Chao Ji,[1] Ying Zhou,[1] Jianli Wang,[1] Fengzhen Huang,[2] and Xiaomei Lu[2,†]

[1]School of Materials Science and Physics, China University of Mining and Technology, Xuzhou 221116, China
[2]National Laboratory of Solid State Microstructures and Physics School, Nanjing University, Nanjing 210093, China

(Received 19 January 2020; revised 12 April 2020; accepted 8 June 2020; published 30 June 2020)

The recent discovery of two-dimensional (2D) ferromagnetism in van der Waals materials has opened the door to the control of 2D magnetism by means of electric field. Here we demonstrate the magnetization reversal through switching polarization in a designed 2D multiferroic oxide by combining group theory analysis and first-principles calculation. We show that ferroelectricity can be induced by a specific octahedral rotation in a perovskite bilayer. Ferromagnetism can be introduced simultaneously by extending the guideline to the B-site ordered double-perovskite bilayer. We have found two coupling mechanisms between polarization and magnetization that enable the reversal of the in-plane magnetization by ferroelectric switching. Our work provides guidelines for the design of 2D multiferroics with intrinsic magnetoelectric coupling and helps to control the 2D magnetism by electric field.

DOI: 10.1103/PhysRevLett.125.017601

The recent discovery of 2D ferromagnetism in van der Waals magnets provides unprecedented opportunities to manipulate magnetism in the 2D limit [1–4]. Electrostatic gate control of magnetism, embodied in electric field-induced modification of magnetic order, saturation magnetization, coercive field and Curie temperature [5–8], has been demonstrated in these 2D ferromagnets. However, electric-field control of magnetization direction, which is a key challenge in the development of the new-generation magnetic memory storage and spintronics [9,10], has not been demonstrated in 2D materials. The coupling between polarization and magnetization in multiferroics may provide an effective way to control the direction of magnetization by electric field [9–12]. Many efforts have been devoted to searching for 2D multiferroics [13–15] since the discovery of 2D ferroelectricity [16–19] and ferromagnetism. However, up to now, the research on 2D multiferroics is mainly focused on van der Waals materials, and the intrinsic magnetoelectric (ME) coupling has not been proposed in these predicted 2D multiferroic materials [15].

Recently, the successful growth of 2D freestanding perovskite oxides [20–22] has stimulated research on the design of 2D functional materials based on perovskite oxides. Octahedral rotation distortion is common in perovskite oxides, which usually tunes the magnetism without breaking the inversion symmetry [23]. However, it has been proposed that in perovskite superlattice [24] and layered perovskites such as the Ruddlesden-Popper (RP) phase [25,26], the combination of two types of octahedral rotation can induce ferroelectricity, which has recently been experimentally demonstrated in RP oxides [27,28]. This suggests that a perovskite bilayer, as the basic building block of the $A_3B_2O_7$-type RP oxides, can induce ferroelectricity through a specific octahedral rotation distortion. However, ferromagnetism is difficult to achieve in a perovskite bilayer because of the common antiferromagnetic (AFM) coupling between neighbor magnetic ions. An effective way to achieve ferromagnetism is to extend the guideline to the B-site ordered double-perovskite (DP) bilayer, in view of the fact that many bulk DP oxides exhibit ferromagnetism or ferrimagnetism with high Curie temperature [29,30]. From the perspective of symmetry, ferroelectricity in this DP bilayer requires oxygen octahedron to form in-phase rotation (IR) and tilt distortion simultaneously, which is the most common form in DP oxides [30]. In addition, a highly ordered DP structure requires a large difference in the valence and radius of the magnetic ions, such as the $3d$-$5d$ combination with B^{3+}/B'^{5+} (or B^{2+}/B'^{6+}) oxidation states. Ferromagnetism or ferrimagnetism has been widely reported in such systems [29,30].

In this Letter, we focus on the DP bilayer with the Fe-Os combination, whose bulk phase Ca_2FeOsO_6 meets the prerequisites of ferroelectricity for octahedral rotation and is a ferrimagnetic insulator [31]. By combining group theory analysis and first-principles calculation, we systematically study the structural, electronic, ferroelectric, and magnetic properties of the Ca_3FeOsO_7 bilayer, as well as the changes of magnetism in ferroelectric switching. We confirm the coexistence of ferroelectricity and ferrimagnetism, and determine the lowest-energy path of reversing polarization. We identify two unique ME coupling mechanisms that

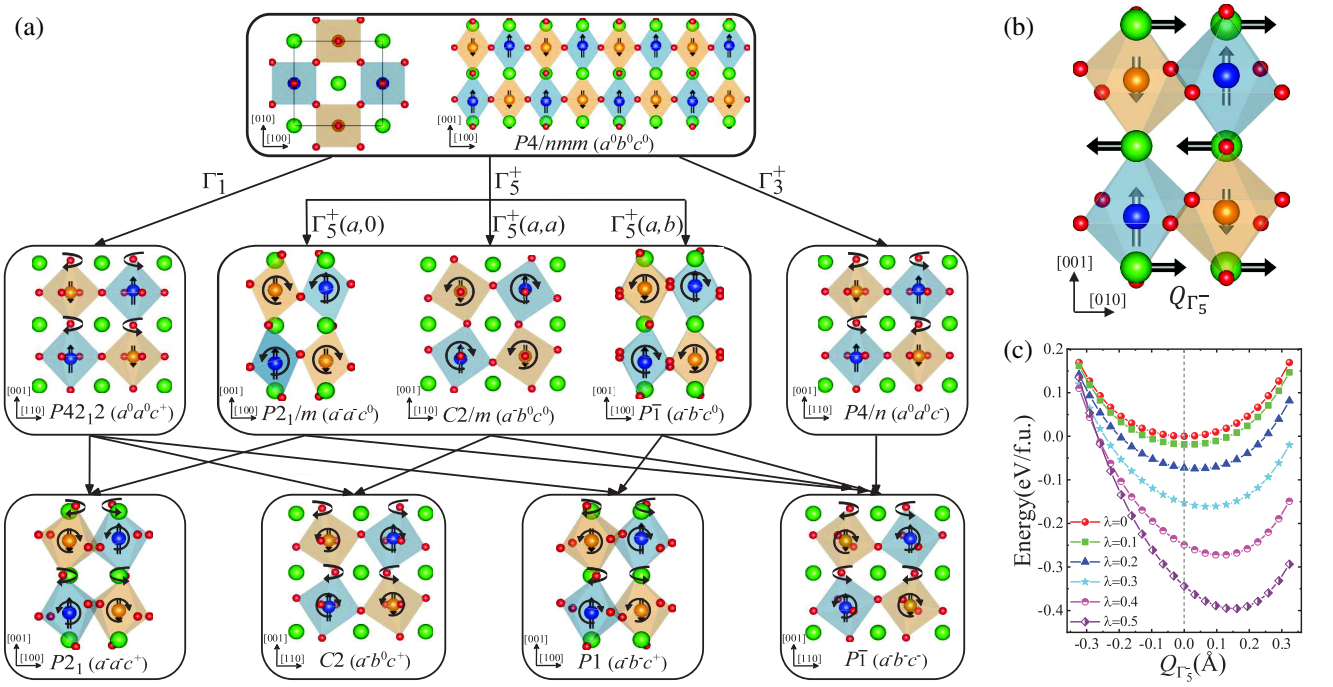

FIG. 1. (a) Crystal structure of the prototype phase of the DP bilayer and the symmetry resulting from various octahedral rotation. (b) The polar mode $Q_{\Gamma_5^-}$ and (c) its coupling with the IR and tilt modes. The change in energy is shown as a function of the amplitude of the polar mode. The parameter λ represents the amplitude of the IR and tilt modes fixed in the calculation.

enable the reversal of the in-plane magnetization through switching polarization.

Ground-state structure.—The B-site ordered DP oxides have a rock-salt-type arrangement of transition-metal ions in the most common case [30], so the prototype phase of its bilayer forms a $\sqrt{2} \times \sqrt{2} \times 2$ perovskite supercell structure with a $P4/nmm$ space group. Group theory analysis shows that there are three types of octahedral rotation: the IR with irreducible representation Γ_1^-, the out-of-phase rotation (OR) with Γ_3^+, and tilt mode with Γ_5^+, as shown in Fig. 1(a). The phonon band structure of the prototype phase [Fig. S1(a) in the Supplemental Material [32]] reveals that the above three types of modes in the Ca_3FeOsO_7 bilayer are all dynamically unstable modes. By contrast, for the Sr_3FeOsO_7 bilayer, only the IR and OR modes are unstable [Fig. S1(b)] [32]. We then calculated the energy gain from freezing each soft mode. The results confirm that only the soft modes involving the three types of octahedral rotation can generate energy gain (Fig. S2 [32]).

Next, we determined the structural symmetries resulting from individual rotation mode and their various combinations [Fig. 1(a)]. The IR plus tilt ($\Gamma_1^- \oplus \Gamma_5^+$) establishes three different polar structures depending on the direction of the tilt axis, while the OR plus tilt ($\Gamma_3^+ \oplus \Gamma_5^+$) results in a nonpolar structure. The ground-state structure of the Ca_3FeOsO_7 bilayer (polar $P2_1$ phase) has the $a^-a^-c^+$ rotation (Table S1 [32]), the same as its bulk phase [31]. Similarly, the $a^0a^0c^-$ rotation pattern of the Sr_3FeOsO_7 bilayer remains unchanged with respect to its bulk phase [31], results in a nonpolar $P4/n$ phase. The dynamic and thermal stability of the ground-state phase in the Ca_3FeOsO_7 bilayer are confirmed by phonon dispersion and *ab initio* molecular dynamics simulation (Fig. S3 and Fig. S4 [32]), respectively. A polar mode dominated by Ca ion displacement emerges in this ground-state phase [Fig. 1(b)]. Its amplitude is proportional to the magnitude of IR and tilt modes [Fig. 1(c)], which is a manifestation of a trilinear coupling [28].

Ferroelectric switching.—Although the combination of IR and tilt modes can establish a polar structure in the absence of the polar distortion, the polar mode is still necessary to maintain such a distorted structure. Figure 2(a) shows the energy landscape around the prototype structure of the Ca_3FeOsO_7 bilayer in the absence of the polar mode. The tilt mode disappears in the lowest-energy structure. When the polar mode is introduced, the IR and tilt modes are both present in the lowest-energy structure [Fig. 2(b)]. Changes in the sign of IR or tilt mode lead to four structural domains. Polarization can be reversed by switching the IR or tilt distortion individually. However, both of these one-step switching paths have an energy barrier too high to reverse polarization. We then considered the two-step switching paths that involves reversing rotation across an antipolar structure [Fig. 3(a)] and reversing tilt via an orthorhombic twin [Fig. 3(b)]. Previous theoretical studies have suggested that these multistep switching paths have lower energy barriers in RP oxides [43,44].

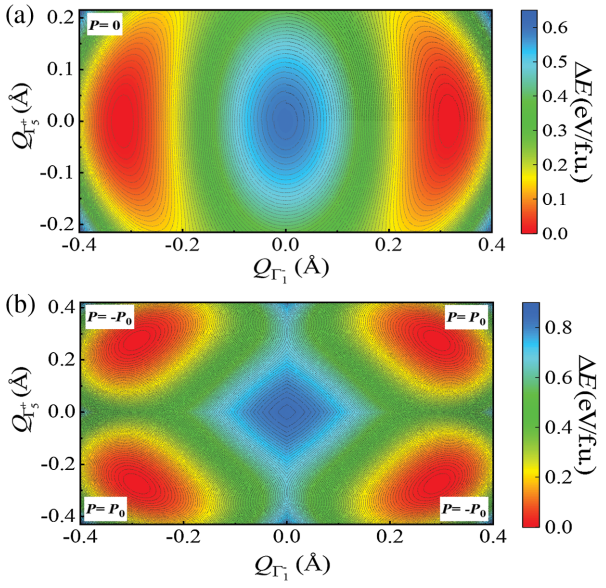

FIG. 2. Total energy as a function of the amplitudes of IR ($Q_{\Gamma_1^-}$) and tilt ($Q_{\Gamma_5^+}$) modes in the (a) absence and (b) presence of the polar mode.

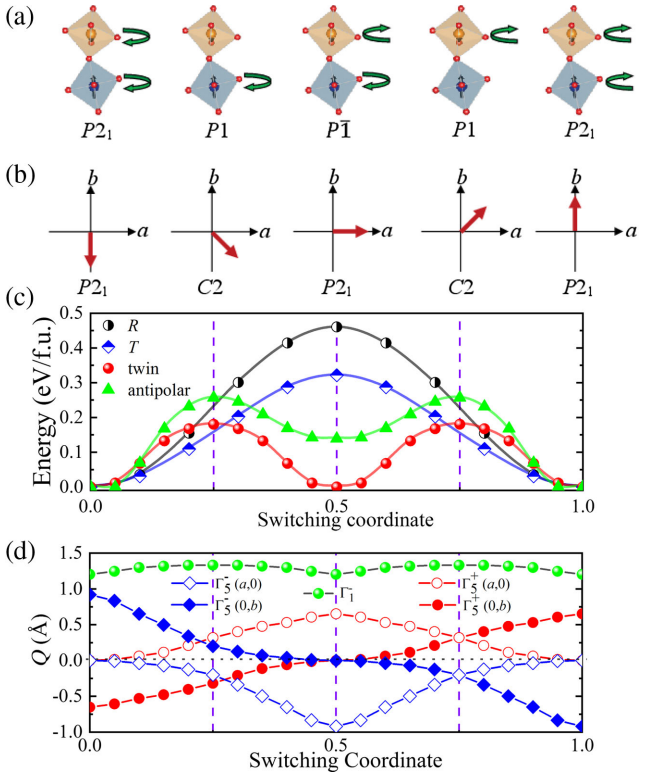

FIG. 3. (a) Schematic of a two-step switching path that reverses the rotation mode. The curved arrow represents the rotation direction of the adjacent octahedron. (b) Schematic of a two-step switching path that reverses the tilt mode. The arrow represents the direction of the tilt axis. (c) Total energy as a function of switching coordinate for one-step switching paths that reverse the rotation (R) or tilt (T) mode, and two-step switching paths via an antipolar or twin structure shown in (a) and (b), respectively. (d) Changes in the decomposed IR (Γ_1^-), tilt (Γ_5^+), and polar (Γ_5^-) modes along the lowest-energy switching path.

We demonstrate that the switching path via an orthorhombic twin has the lowest energy barrier [Fig. 3(c)], about twice the calculated value of $Ca_3Ti_2O_7$ [43]. Correspondingly, its ferroelectric polarization reaches ~31 $\mu C/cm^2$ (expressed in bulk form by considering its thickness), greater than that of the latter. The variation of each distortion mode along this lowest-energy switching path [Fig. 3(d)] confirms that the tilt axis and polarization undergo a 180° rotation in the ab plane.

Reversal of magnetization through switching polarization.—Electronic structure calculation (Fig. S5 [32]) confirms the $Fe^{3+}(3d^5)$ and $Os^{5+}(5d^3)$ electronic configurations and semiconductor property of this ferroelectric phase. The calculation of the total energy of various magnetic orderings (Fig. S6 [32]) shows that the magnetic ground state exhibits a G-type AFM order (i.e., ferrimagnetism), identical to its bulk phase. The Monte Carlo simulation further confirms the magnetic ground state and estimates its Curie temperature to be ~210 K (Fig. S7 [32]). These results confirm that the Ca_3FeOsO_7 bilayer is a 2D multiferroic material. Then we studied the evolution of magnetism in ferroelectric switching. A magnetic phase transition from G-type to C-type phase emerges in ferroelectric switching (Fig. S6 [32]). This transition is similar to the change in the magnetic phase from the G type of Ca_2FeOsO_6 to the C-type phase of Sr_2FeOsO_6 [31]. It can be attributed to the change in the competition between the AFM exchange interactions of the out-of-plane Fe-Os and Os-Os bonds, which show opposite trends with the change of tilt distortion (Fig. S8 [32]).

Magnetic anisotropy calculation [Fig. 4(a)] shows that the easy-magnetization axis always lies in the plane perpendicular to the polarization. Although the Dzyaloshinskii-Moriya (DM) interaction [45,46] results in a canted spin configuration and contributes to magnetic anisotropy, the easy-axis direction changes slightly when the DM interaction is included (Fig. S9 [32]). This ME coupling is similar to that of multiferroic $BiFeO_3$, whose AFM plane is always perpendicular to the polarization [47]. What is different, however, is that in the Ca_3FeOsO_7 bilayer the reversal of the polarization results in a change in the easy-axis direction. The easy axis turns to a direction symmetric about the c axis with respect to its initial direction [Fig. 4(a)]. There are two possible paths of switching magnetization as polarization reverses, which lead to the reversal of the in-plane and out-of-plane magnetization, respectively [Fig. 4(b)]. The actual path depends on the evolution of the easy-axis direction in the process of ferroelectric switching. Figure 4(c) shows the magnetic anisotropy energy surface of a series of intermediate structures during the transition from the initial state to the orthogonal twin state. From the second step, the easy axis turns to the direction

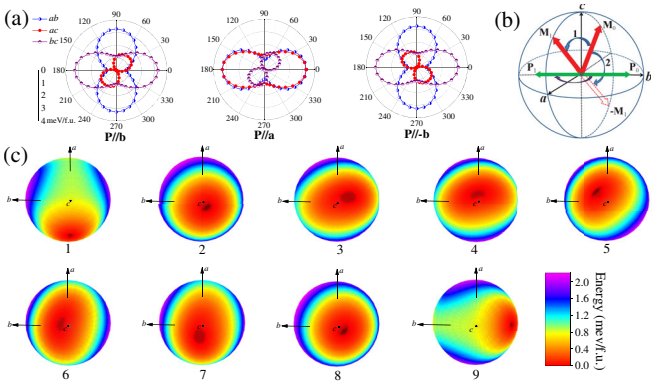

FIG. 4. (a) Magnetic anisotropy energy of the initial ($\mathbf{P}//\mathbf{b}$), orthogonal twin ($\mathbf{P}//\mathbf{a}$), and final ($\mathbf{P}//-\mathbf{b}$) states in ferroelectric switching, where $\mathbf{P}$ represents the ferroelectric polarization. The change in energy is shown as a function of the angle between the spin direction and the basis vector. When the spins lie in the ab (ac) and bc planes, the angle refers to the a and b axes, respectively. (b) Schematic of the change in the magnetization direction with the reversal of polarization. (c) Magnetic anisotropy energy surface of a series of intermediate structures along the switching path from the initial state to the orthogonal twin state.

close to the c axis, and rotates continuously around the c axis. This significant change with respect to the initial state is related to the aforementioned magnetic phase transition. These results demonstrate that the magnetization direction always changes in the upper hemisphere without crossing the ab plane, so the in-plane magnetization will be reversed in ferroelectric switching.

Epitaxial strain is known to have a significant effect on octahedral rotation in perovskite films [23]. By combining the strain-bulk and heterostructure models, we studied the effect of epitaxial strain and interface hybridization on this bilayer. For the heterostructure model, we chose the most commonly used $SrTiO_3$ substrate. The results show that there is no obvious hybridization at the interface, and the interface effect does not change the ground-state structural, ferroelectric and magnetic properties (Fig. S10 [32]). The ferroelectric $P2_1$ phase is always the ground state over the entire strain range (Fig. S11 [32]). However, the energy barrier of reversing tilt distortion in one or two steps is significantly reduced by compressive strain, which is related to the suppression of tilt distortion by compressive strain. The switching path via an orthorhombic twin still has the lowest energy barrier of 79 meV/f.u., (Fig. S11 [32]) slightly lower than that of $Ca_3Ti_2O_7$ [43].

The compressive strain also causes the transition of magnetic phase from G-type to C-type AFM order. However, spin canting induced by DM interaction results in weak ferromagnetism with a considerable net magnetization (0.38 μ_B/f.u.). Phenomenologically the DM interaction can be described by [48]

$$E_{\mathrm{DM}} = \mathbf{D} \cdot (\mathbf{L} \times \mathbf{M}),$$

where $\mathbf{D}$ is the total DM vector, $\mathbf{L}$ is the AFM vector representing the spin direction, and $\mathbf{M}$ is the net magnetization. According to this expression, reversing $\mathbf{D}$ or $\mathbf{L}$ individually will cause the reversal of $\mathbf{M}$. Therefore, if the $\mathbf{D}$ vector is coupled to ferroelectric distortion and $\mathbf{L}$ remains unchanged in ferroelectric switching, the reversal of magnetization can be achieved by means of DM interaction. This mechanism has been proposed in some multiferroic materials [25,48]. However, the difference is that for the Ca_3FeOsO_7 bilayer, both $\mathbf{D}$ and $\mathbf{L}$ vectors are coupled with octahedral rotation, suggesting a more complex coupling mechanism.

Figure 5(a) shows the transformation of the DM vectors of the in-plane nearest-neighbor bonds caused by the reversal of rotation or tilt distortion. Symmetry analysis and first-principles calculations demonstrate that the reverse of tilt inverts the in-plane component of $\mathbf{D}$ vector with the out-of-plane component D_z unchanged (Fig. S12 [32]), while reversing the rotation distortion causes the components perpendicular to tilt axis to be reversed, as depicted in Fig. S13 [32]. In the C-type AFM structure, the component of the $\mathbf{D}$ vector parallel to the polarization disappears in the sum of all DM interactions. This causes $\mathbf{L}$ to be oriented along the direction of polarization, which has

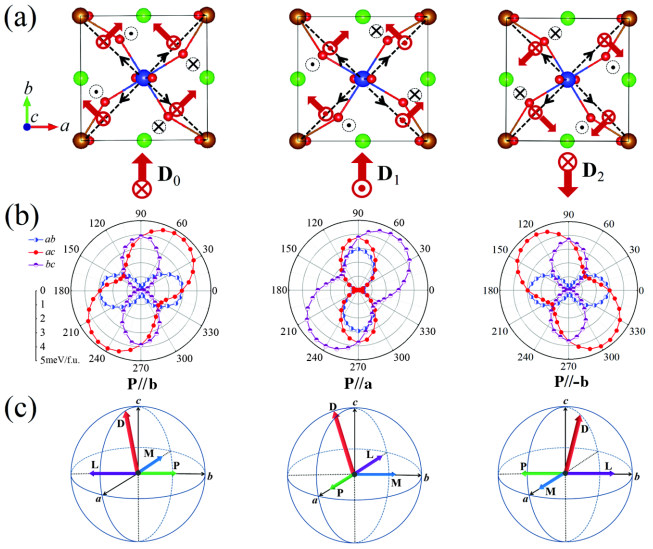

FIG. 5. (a) The orientation of the DM vector of each in-plane nearest-neighbor bond and the total vectors for the sum (denoted by $\mathbf{D}_0$-$\mathbf{D}_2$). The middle and right images represent their transformations caused by the reversal of rotation and tilt distortion, respectively. The red arrows represent the orientation of the DM vector, while the black vertical arrows represent the displacement of adjacent O ions caused by tilt distortion. (b) Magnetic anisotropy energy including DM interaction at −2% compressive strain and (c) schematic of the orientations of the DM vector $\mathbf{D}$, AFM vector $\mathbf{L}$, and net magnetization $\mathbf{M}$ for the initial, intermediate, and final states.

been confirmed by the magnetic anisotropy calculation [Fig. 5(b)]. The dominant D_z component causes **M** to lie mainly in the ab plane perpendicular to the polarization [Fig. 5(c)]. In ferroelectric switching, the continuous change of the in-plane component of the **D** vector (Fig. S12 [32]) causes the reverse of the **L** vector, while the D_z component is unchanged, resulting in the reversal of **M**, as shown in Fig. 5(c).

In conclusion, we propose the design of 2D multiferroic materials with intrinsic ME coupling based on DP oxides. The design principles can be summarized as the combination of the ferroelectricity induced by octahedral rotation and the ferromagnetism (or ferrimagnetism) caused by the ordered arrangement of different magnetic ions in 2D perovskite oxides. Ferroelectricity requires octahedra to form IR and tilt distortion with appropriate amplitude. Ferromagnetism (or ferrimagnetism) can be introduced simultaneously by designing combinations of magnetic ions with large difference in ionic radius and valence, such as the $3d$-$5d$ combination. The strong spin-orbital coupling of $5d$ electrons can generate large magnetic anisotropy to stabilize the 2D ferromagnetism, and may induce large net magnetic moment even in AFM structure. We have found two ME coupling mechanisms that enable the reversal of magnetization through ferroelectric switching, which, respectively, depend the change in the easy-axis direction and the rotation of the DM vector caused by the reversal of tilt distortion.

This work was financially supported by the National Key Research Program of China (Grant No. 2016YFA0201004), National Natural Science Foundation of China (Grants No. 11974418, No. 11874208, and No. 11804383), and the Fundamental Research Funds for the Central Universities (Grant No. 2019QNA30). Computer resources provided by the High Performance Computing Center of Nanjing University are gratefully acknowledged.

*juntingzhang@cumt.edu.cn
†xiaomeil@nju.edu.cn

[1] C. Gong, L. Li, Z. L. Li, H. W. Ji, A. Stern, Y. Xia, T. Cao, W. Bao, C. Z. Wang, Y. A. Wang *et al.*, Nature (London) **546**, 265 (2017).
[2] B. Huang, G. Clark, E. Navarro-Moratalla, D. R. Klein, R. Cheng, K. L. Seyler, D. Zhong, E. Schmidgall, M. A. McGuire, D. H. Cobden *et al.*, Nature (London) **546**, 270 (2017).
[3] Y. J. Deng, Y. J. Yu, Y. C. Song, J. Z. Zhang, N. Z. Wang, Z. Y. Sun, Y. F. Yi, Y. Z. Wu, S. W. Wu, J. Y. Zhu *et al.*, Nature (London) **563**, 94 (2018).
[4] M. Bonilla, S. Kolekar, Y. J. Ma, H. C. Diaz, V. Kalappattil, R. Das, T. Eggers, H. R. Gutierrez, M. H. Phan, and M. Batzill, Nat. Nanotechnol. **13**, 289 (2018).
[5] B. Huang, G. Clark, D. R. Klein, D. MacNeill, E. Navarro-Moratalla, K. L. Seyler, N. Wilson, M. A. McGuire, D. H. Cobden, D. Xiao *et al.*, Nat. Nanotechnol. **13**, 544 (2018).
[6] S. W. Jiang, L. Z. Li, Z. F. Wang, K. F. Mak, and J. Shan, Nat. Nanotechnol. **13**, 549 (2018).
[7] S. W. Jiang, J. Shan, and K. F. Mak, Nat. Mater. **17**, 406 (2018).
[8] Z. Wang, T. Y. Zhang, M. Ding, B. J. Dong, Y. X. Li, M. L. Chen, X. X. Li, J. Q. Huang, H. W. Wang, X. T. Zhao *et al.*, Nat. Nanotechnol. **13**, 554 (2018).
[9] F. Matsukura, Y. Tokura, and H. Ohno, Nat. Nanotechnol. **10**, 209 (2015).
[10] A. C. Garcia-Castro, W. Ibarra-Hernandez, E. Bousquet, and A. H. Romero, Phys. Rev. Lett. **121**, 117601 (2018).
[11] L. Chen, C. S. Xu, H. Tian, H. J. Xiang, J. Iniguez, Y. R. Yang, and L. Bellaiche, Phys. Rev. Lett. **122**, 247701 (2019).
[12] N. A. Spaldin and R. Ramesh, Nat. Mater. **18**, 203 (2019).
[13] C. X. Huang, Y. P. Du, H. P. Wu, H. J. Xiang, K. M. Deng, and E. J. Kan, Phys. Rev. Lett. **120**, 147601 (2018).
[14] J. S. Qi, H. Wang, X. F. Chen, and X. F. Qian, Appl. Phys. Lett. **113**, 043102 (2018).
[15] T. Hu and E. J. Kan, Comput. Mol. Sci. **9**, e1409 (2019).
[16] K. Chang, J. W. Liu, H. C. Lin, N. Wang, K. Zhao, A. M. Zhang, F. Jin, Y. Zhong, X. P. Hu, W. H. Duan *et al.*, Science **353**, 274 (2016).
[17] F. C. Liu, L. You, K. L. Seyler, X. B. Li, P. Yu, J. H. Lin, X. W. Wang, J. D. Zhou, H. Wang, H. Y. He *et al.*, Nat. Commun. **7**, 12357 (2016).
[18] Y. Zhou, D. Wu, Y. H. Zhu, Y. J. Cho, Q. He, X. Yang, K. Herrera, Z. D. Chu, Y. Han, M. C. Downer *et al.*, Nano Lett. **17**, 5508 (2017).
[19] Z. Y. Fei, W. J. Zhao, T. A. Palomaki, B. S. Sun, M. K. Miller, Z. Y. Zhao, J. Q. Yan, X. D. Xu, and D. H. Cobden, Nature (London) **560**, 336 (2018).
[20] D. Lu, D. T. Baek, S. S. Hong, L. F. Kourkoutis, Y. Hikita, and H. Y. Hwang, Nat. Mater. **15**, 1255 (2016).
[21] S. S. Hong, J. H. Yu, D. Lu, A. F. Marshall, Y. Hikita, Y. Cui, and H. Y. Hwang, Sci. Adv. **3**, eaao5173 (2017).
[22] D. X. Ji, S. H. Cai, T. R. Paudel, H. Y. Sun, C. C. Zhang, L. Han, Y. F. Wei, Y. P. Zang, M. Gu, Y. Zhang *et al.*, Nature (London) **570**, 87 (2019).
[23] J. M. Rondinelli, S. J. May, and J. W. Freeland, MRS Bull. **37**, 261 (2012).
[24] J. M. Rondinelli and C. J. Fennie, Adv. Mater. **24**, 1961 (2012).
[25] N. A. Benedek and C. J. Fennie, Phys. Rev. Lett. **106**, 107204 (2011).
[26] A. T. Mulder, N. A. Benedek, J. M. Rondinelli, and C. J. Fennie, Adv. Funct. Mater. **23**, 4810 (2013).
[27] Y. S. Oh, X. Luo, F. T. Huang, Y. Z. Wang, and S. W. Cheong, Nat. Mater. **14**, 407 (2015).
[28] S. Yoshida, K. Fujita, H. Akamatsu, O. Hernandez, A. S. Gupta, F. G. Brown, H. Padmanabhan, A. S. Gibbs, T. Kuge, R. Tsuji *et al.*, Adv. Funct. Mater. **28**, 1801856 (2018).
[29] D. Serrate, J. M. D. Teresa, and M. R. Ibarra, J. Phys. Condens. Matter **19**, 023201 (2007).
[30] S. Vasala and M. Karppinen, Prog. Solid State Chem. **43**, 1 (2015).
[31] H. L. Feng, M. Arai, Y. Matsushita, Y. Tsujimoto, Y. F. Guo, C. I. Sathish, X. Wang, Y. H. Yuan, M. Tanaka, and K. Yamaura, J. Am. Chem. Soc. **136**, 3326 (2014).

[32] See the Supplemental Material at http://link.aps.org/supplemental/10.1103/PhysRevLett.125.017601 for more computational details and results about the phonon dispersions, energy gain, molecular dynamics simulations, projected band structures, magnetic ground state, magnetic exchange interaction, Monte Carlo simulations, magnetic anisotropy, strain effect, and DM interaction, which includes Refs. [33–42].
[33] P. E. Blöchl, Phys. Rev. B **50**, 17953 (1994).
[34] G. Kresse and J. Furthmüller, Phys. Rev. B **54**, 11169 (1996).
[35] J. P. Perdew, A. Ruzsinszky, G. I. Csonka, O. A. Vydrov, G. E. Scuseria, L. A. Constantin, X. L. Zhou, and K. Burke, Phys. Rev. Lett. **100**, 136406 (2008).
[36] S. L. Dudarev, G. A. Botton, S. Y. Savrasov, C. J. Humphreys, and A. P. Sutton, Phys. Rev. B **57**, 1505 (1998).
[37] H. Wang, S. Zhu, X. Ou, and H. Wu, Phys. Rev. B **90**, 054406 (2014).
[38] A. Togo and I. Tanaka, Scr. Mater. **108**, 1 (2015).
[39] D. Sheppard, P. Xiao, W. Chemelewski, D. D. Johnson, and G. Henkelman, J. Chem. Phys. **136**, 074103 (2012).
[40] R. D. King-Smith and D. Vanderbilt, Phys. Rev. B **47**, 1651 (1993).
[41] B. J. Campbell, H. T. Stokes, D. E. Tanner, and D. M. Hatch, J. Appl. Crystallogr. **39**, 607 (2006).
[42] I. A. Sergienko and E. Dagotto, Phys. Rev. B **73**, 094434 (2006).
[43] E. A. Nowadnick and C. J. Fennie, Phys. Rev. B **94**, 104105 (2016).
[44] J. M. Munro, H. Akamatsu, H. Padmanabhan, V. S. Liu, Y. Shi, L. Q. Chen, B. K. VanLeeuwen, I. Dabo, and V. Gopalan, Phys. Rev. B **98**, 085107 (2018).
[45] I. Dzyaloshinsky, J. Phys. Chem. Solids **4**, 241 (1958).
[46] T. Moriya, Phys. Rev. **120**, 91 (1960).
[47] T. Zhao, A. Scholl, F. Zavaliche, K. Lee, M. Barry, A. Doran, M. P. Cruz, Y. H. Chu, C. Ederer, N. A. Spaldin *et al.*, Nat. Mater. **5**, 823 (2006).
[48] C. J. Fennie, Phys. Rev. Lett. **100**, 167203 (2008).